JMEPEG (2009) 18:174–181
DOI: 10.1007/s11665-008-9285-6

1059-9495/$19.00

Microstructural Modifications of As-Cast High-Chromium White Iron by Heat Treatment

A.E. Karantzalis, A. Lekatou, and H. Mavros

(Submitted June 5, 2008)

The initial as-cast microstructure of a high-chromium (2.35% C, 18.23% Cr) white cast iron consisting of primary austenitic dendrites and a eutectic mixture of M_7C_3 carbides/austenite was extensively modified by four different heat treatments: H.T.A: destabilization (970 °C-2.5 h), H.T.B: destabilization/subcritical treatments (970 °C-2.5 h + 600 °C-13 h), H.T.C: subcritical treatment (600 °C-13 h) and H.T.D: subcritical/destabilization treatments (600 °C-13 h + 970 °C-2.5 h). H.T.A leads to martensitic structures that present considerable precipitation of cubic secondary carbide particles of $M_{23}C_6$ type. H.T.B produces pearlitic structures and causes further carbide precipitation and pre-existent carbide particle shape modifications. H.T.C extensively modifies the initial as-cast structure to more pearlitic morphologies accompanied with spheroidization/degradation of the M_7C_3 primary carbide structure. H.T.D causes extensive formation of secondary carbide particles within the primary austenitic matrix; the latter has been mainly transformed to martensite. The effect of each heat treatment on the hardness of the alloy was correlated with the attained microstructure.

Keywords cast irons, heat treating, modification

1. Introduction

High-chromium white irons are extensively used in applications where good resistance to abrasion wear is required, for example mineral processing, cement manufacturing, and slurry pumping (Ref 1-3). This attractive wear behavior is clearly attributed to the microstructure and the participating phases, both in the as-cast and after heat treatment conditions. Tabrett et al. (Ref 1) in their extensive review, address all the different parameters that affect the final microstructure of these materials. Especially, as far as the wear behavior is concerned, the matrix, the secondary and the primary carbide phases are responsible for the abrasion wear resistance of such alloys, with latter being the most significant one (Ref 1). Martensitic phases are considered to have a positive effect on the wear resistance, whereas pearlitic/ferritic morphologies generally increase the wear loss (Ref 1-4, 6, 8). Austenitic matrices have led to contradicting results due to the extensive work hardening effect that accordingly influence their wear behavior (Ref 1, 2, 4, 8). The effect of secondary carbide presence should be examined along with other parameters, such as wear conditions, environment, abrasive media, etc. (Ref 1, 4).

The initial structure of the as-cast alloy essentially consists of an austenitic dendritic matrix and a eutectic mixture of austenite/M_7C_3. This primary morphology can be significantly transformed through different critical and subcritical heat treatments. The scope of the heat treatments is generally the precipitation of secondary carbide particles accompanied by a simultaneous austenite destabilization and its transformation to other phases, most desirably martensite. Critical (destabilization) heat treatments are conducted at 920-1060 °C, for 1-6 h (Ref 1-10). Subcritical treatments usually follow the destabilization treatments. They are conducted at 200-600 °C for 2-6 h (Ref 1-10). Several research efforts have investigated the effect of such treatments on the wear behavior of high-chromium white irons, the detailed presentation of which would be out of the scope of this work. For further information, the reader should address to relative literature (Ref 1-10).

Various research works have been focused on the formation, the morphology, and the characteristics of the secondary carbide particles formed during critical and subcritical treatments of high-chromium white irons. The work of Asensio et al. (Ref 11) could be a very useful primary approach on the expected—according to the chemical composition of the alloy—matrix, primary and secondary carbide phases. Wang et al. (Ref 12) studied the precipitation and transformation of secondary carbides in a 16Cr-1Mo-1Cu cast iron subjected to a destabilization heat treatment. They concluded that two types of $(Fe,Cr)_{23}C_6$ secondary carbide particles have precipitated: One of cubic morphology with a specific orientation relative to the matrix and one of grainy morphology with no specific orientation. The latter had most likely been formed during the cooling stage of the destabilization process. They also observed that after prolonged holding times, the $(Fe,Cr)_{23}C_6$ particles had been transformed into M_7C_3 rods. The same researchers (Ref 13) investigated the influence of a subcritical heat treatment on a 14Cr-1Mo-1.5 V cast iron. Two hardening maxima were observed, as a result of this treatment: The first one—at relatively early stages—was mainly associated with the formation of both martensite and $(Fe,Cr)_{23}C_6$; The second one was mainly associated with the formation of MoC and $(Cr,V)_2C$ and/or the transformation of

A.E. Karantzalis, A. Lekatou, and **H. Mavros**, Department of Materials Science and Engineering, University of Ioannina, 45110 Ioannina, Greece. Contact e-mails: alekatou@cc.uoi.gr, alexkarantzalis@gmail.com and dreznas@yahoo.gr.

$M_{23}C_6$ to the above carbides. According to their observations, prolonged holding at a subcritical temperature causes dissociation of $M_{23}C_6$ to M_3C accompanied by pearlite formation with a subsequent decrease in the bulk hardness. Zhang et al. (Ref 14) verified the formation of secondary carbide particles after subcritical heat treatments of two chromium cast irons of different Cr content. Powell and Bee (Ref 15), in the work on destabilizing a 18% Cr white iron, reported that cuboid $M_{23}C_6$ particles had precipitated within the austenitic matrix after a short time at the destabilization temperature (1273 °K); After 4 h at the same temperatures a mixture of $M_{23}C_6$ and M_7C_3 had been formed. They also noted the formation of secondary carbide particles at the sub-grain boundaries during the solidification stage. Powell and Laird (Ref 16) investigated the effects of the Cr content and destabilization heat treatments on the structure, growth, and morphology of secondary carbides. As the Cr content increased, the tendency for the secondary carbide stoichiometry followed the sequence M_3C, M_7C_3, and $M_{23}C_6$. None of the carbides showed any preferential tendency to form/grow from the eutectic carbide phase. In all cases, the secondary carbide particles have been developed within the austenitic matrix with their morphological features varying from plate-like for M_3C to rod-shaped for the M_7C_3 and fibrous-like for $M_{23}C_6$. Similar observations on the topology and morphology of secondary carbide precipitation were made by Wiengmoon et al. (Ref 17), who dealt with 30% Cr white irons. Carpenter and Carpenter (Ref 18), by employing XRD analytical techniques, addressed the issue of the eutectic carbide stability in relation to the destabilization treatment. They verified previously stated hypothesis (Ref 19-21) regarding the eutectic M_7C_3 transformation to $M_{23}C_6$. Carpenter et al. (Ref 22), using XRD analysis, identified the secondary carbide particles formed in the austenitic matrix of a destabilized 27% Cr white iron, as of the $(Fe,Cr)_{23}C_6$ type. Sun et al. (Ref 23) studying the effect of subcritical heat treatments on a 16Cr-1Mo-1Cu cast iron with TEM, observed a certain sequence of secondary carbide formation/transformation according to the holding time. Thus, treatment of 10 h at 853 °K resulted in the presence of $(Fe,Cr)_{23}C_6$; 16 h at 853 °K led to the precipitation of MoC, Fe_2MoC, and ε-carbide; 23 h at 853 °K led to the formation/transformation of M_3C.

The vast majority of experimental efforts have applied the sequence of casting, destabilization heat treatment and finally subcritical heat treatment. The present work applies the opposite route, i.e., casting—subcritical heat treatment—destabilization with the aim to explore all the possibilities for a close control of the microstructure and subsequently crucial properties. This effort is specifically focused on the shape, morphology, topology, stoichiometry, and distribution of the primary (eutectic) and secondary carbide particles as these parameters can have a significant effect on the mechanical properties (hardness, toughness, etc.) and the wear resistance of these alloys family.

2. Experimental Procedure

The cast chromium white iron examined in this work contained 2.35% C, 0.61% Si, 0.62% Mn, 18.23% Cr, 0.58% Mo, 0.35% Ni, 0.46% Cu, and 0.028% P, Fe-balanced. The material was prepared by induction of appropriate raw material.

Table 1 The four different heat treatments the alloy was subjected to

Heat treatment	Description
H.T.A	Heating at 970 °C for 2.5 h-air cooled
H.T.B	Heating at 970 °C for 2.5 h-air cooled Heating at 600 °C for 13 h-air cooled
H.T.C	Heating at 600 °C for 13 h-air cooled
H.T.D	Heating at 600 °C for 13 h-air cooled Heating at 970 °C for 2.5 h-air cooled

Table 2 Microstructure and hardness of the alloys at the five states

State	Microstructure	Hardness HRC
As cast	γ—dendrites, eutectic M_7C_3/γ, martensite layer surrounding M_7C_3	50 ± 3
H.T.A	Martensite, primary M_7C_3, cuboid secondary $M_{23}C_6$, pearlite	66 ± 3
H.T.B	Pearlite, primary M_7C_3, coarse/spheroidized M_7C_3, medium size cuboid $M_{23}C_6$, fine carbide particles	55 ± 4
H.T.C	Pearlite, α-ferrite, spheroidized M_xC_3 particles (x slightly > 7)	43 ± 5
H.T.D	Martensite, primary M_7C_3, secondary spherical M_7C_3, retained γ	62 ± 4

Casting was then conducted from 1440 to 1460 °C into bentonite sand molds. Specimens were cut off and subjected to the heat treatments shown in Table 1.

Specimens were mounted, ground, and polished following standard metallographic procedure and chemically etched by of 10wt.% ammonium persulfate aqueous solution. Hardness (HRC) was measured by a portable hardness tester (brand Equotip). XRD measurements were performed in a Bruker D8 Advance X-ray powder diffractometer equipped with a secondary graphite monochromator and Cu-Ka lamp with λ = 1.48 Å. SEM inspection was carried out using a Zeiss SUPRA 35VP SEM with field emission gun, equipped with a Roentec Quantax (Bruker AXs) EDS system.

3. Results and Discussion

The microstructures resulted from casting and the four different heat treatments are outlined in Table 2.

3.1 As-Cast State

The microstructure of cast iron is illustrated in Fig. 1. The overall microstructural appearance seems to be in agreement with previous works (Ref 1-10). The identified morphologies are large austenite dendrites surrounded by a eutectic mixture of carbide particles (usually acicular) and austenite. These observations are also in agreement with the predicted phases in the iron-rich corner of the ternary Fe-Cr-C phase diagram (Ref 1, 7). The solidification sequence of such alloys (hypoeutectic) has been clarified by several researchers (Ref 2-10) and finally summarized by Tabrett et al. (Ref 1). According to this sequence, solidification commences with the formation of

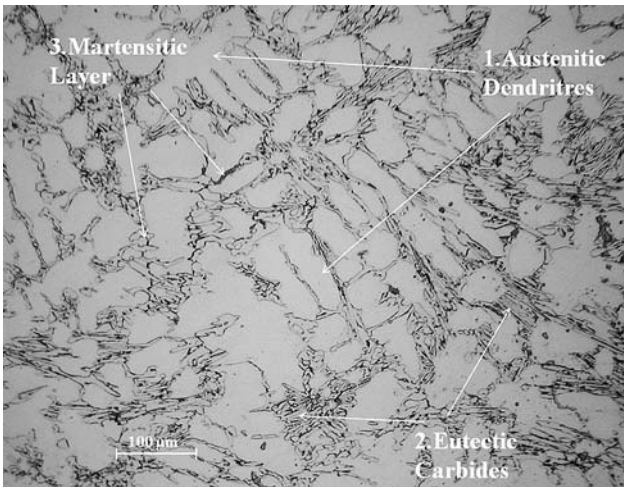

Fig. 1 Optical micrograph of the as-cast alloy. 1: Austenitic dendrites, 2: M_7C_3 eutectic carbides, 3: Martensitic layer

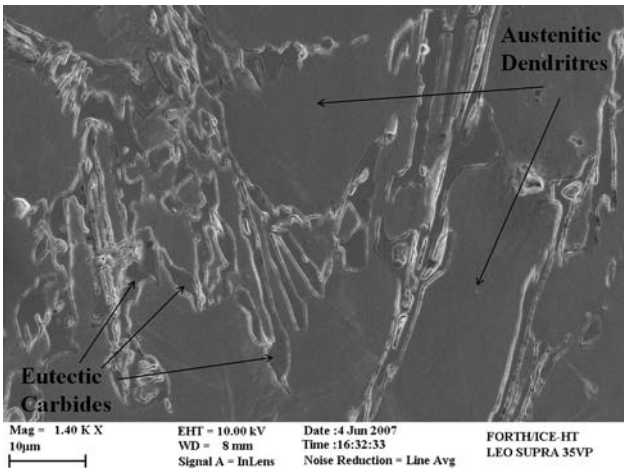

Fig. 2 SEM micrograph of the as-cast alloy showing large acicular plates of eutectic M_7C_3 embedded in an austenitic matrix

austenite dendrites. As temperature decreases, the remaining liquid approaches the eutectic temperature where the eutectic mixture of M_7C_3 and austenite is formed. Further decrease in temperature to ambient temperature leads to metastable austenite retaining. This retaining has been attributed to the presence of high contents of alloying elements and carbon that can inhibit pearlite formation and decrease the martensite start temperature M_s below zero (Ref 1).

Closer examination of Fig. 1 reveals that the eutectic carbide particles are surrounded by a thin dark layer. The dark layer has been associated with the formation of martensite (Ref 1-7). It is postulated that the formation of the eutectic carbides in contact with the primary austenitic phase has consequently led to the excessive consumption and, therefore, matrix depletion of C and Cr. Consequently, the M_s temperature at this localized interfacial regime has increased. As a result, martensite has formed at the periphery of the primary carbide particles. The main microstructural features, in higher magnification, are shown in Fig. 2 where large acicular eutectic carbide particles are surrounded by the austenitic matrix.

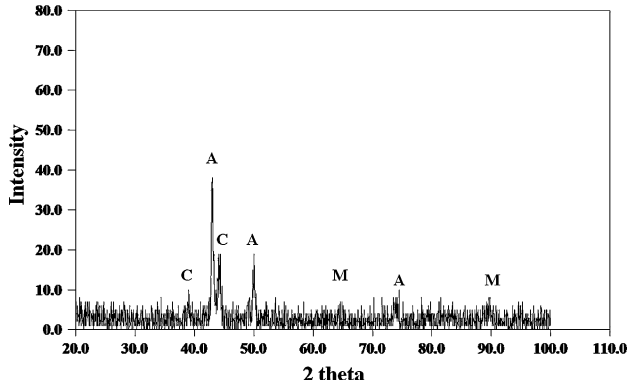

Fig. 3 XRD spectrum of the as-cast alloy. A: austenite, C: M_7C_3, M: martensite

EDX analysis of the carbide phase revealed compositions that approach the M_7C_3 stoichiometry. These observations are also supported by the XRD spectrum of Fig. 3 where austenite, M_7C_3 and limited, yet not negligible, martensite are the identified phases. The identification of M_7C_3 is also based on EDX due to peak overlapping of the M_xC_y carbides such as M_7C_3, $M_{23}C_6$, M_6C, etc.). Here, it should be mentioned, that no secondary carbide formation, as observed in other research instances (Ref 15), was observed. Hardness measurements for the as-cast material provided an average of the order of 50 ± 3 HRC, which is in accordance with other experimental measurements for such alloys (Ref 5, 13).

3.2 Heat Treatment A

Heating of the alloy at 970 °C (H.T.A.) has caused drastic changes in the microstructure. Figure 4 presents the resulting microstructure mainly comprising of large islands of the characteristic inner needle-like morphology along with acicular eutectic carbide particles. The observed microstructural features have also been identified by previous studies (Ref 6-10). The mechanism of martensitic transformation for these specific alloys is well established (Ref 1, 5-12). In this work, apart from these phases, some pearlitic morphologies can also be distinguished, attributed to locally lower cooling rates. Further examination with SEM (Fig. 5 and 6) reveals the extensive formation of secondary carbides within the martensitic matrix. These secondary carbides have a strictly defined cuboid morphology, while their precipitation seems to follow a specific grit-like pattern. EDX analysis revealed that the secondary carbides have stoichiometries close to $M_{23}C_6$. There is no preferential association of the secondary carbide precipitation with the eutectic carbide phase, while they are almost entirely located within the martensitic colonies. These observations are in compatibility with other works (Ref 12-23), where various mechanisms of precipitation are proposed. Particularly, in the research effort of Powell and Bee (Ref 15), the morphology, shape and preferential orientation of the secondary carbide phase are almost identical with the characteristics observed in this work. Powell and Bee explained the thermodynamically unfavorable formation of $M_{23}C_6$, in terms of crystallographic matching between the lattice parameters of the carbide and the cubic matrix crystal structure. Such a matching lowers the activation energy that is essential for nucleation and, thus, reduces the overall involved surface energy.

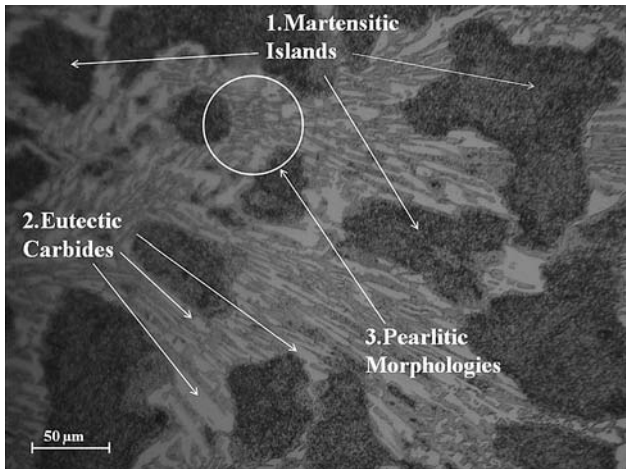

Fig. 4 Optical micrograph showing the microstructure of the alloy after H.T.A. 1: Martensitic matrix, 2: Eutectic carbide particles, 3. Pearlitic morphologies

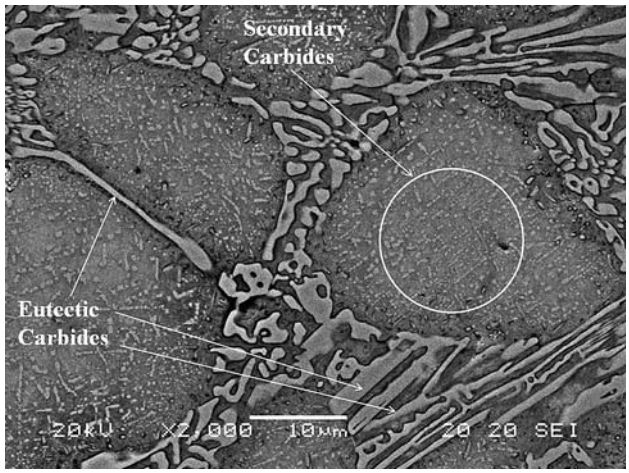

Fig. 5 SEM micrograph of the alloy after H.T.A showing excessive secondary carbide formation within the matrix is shown

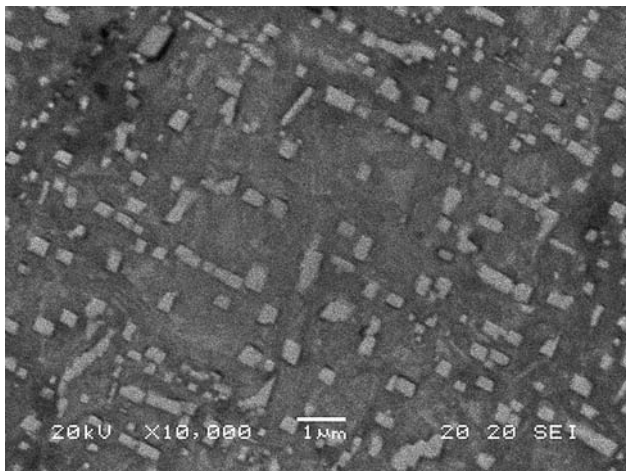

Fig. 6 Details of the circled area in Fig. 5 illustrating the cubic morphology of the secondary carbide particles. Their alignments almost form a grit-like pattern

Hardness measurements gave values of 66 ± 3 HRC. The martensite formation and secondary carbide precipitation are the predominant reasons for such an increase (Ref 1-6, 8, 13, 14). Such a microstructure is also reported to have a favoring effect on the abrasion wear resistance (Ref 1-8).

3.3 Heat Treatment B

Figure 7 illustrates the microstructure of the destabilized and quenched specimen after annealing (H.T.B). It is easily seen that this specific heat treatment has caused significant modifications not only to the microstructure after H.T.A, but also to the microstructure of the as-cast material. The microstructure consists of large ferritic grains, eutectic carbide particles, and pearlitic structures. Closer examination of the ferritic grains (Fig. 8 and 9) reveals a massive precipitation of secondary carbides, which have been formed either during H.T.A or during the subsequent annealing. As shown in Fig. 9, the secondary carbide particles can be classified into three

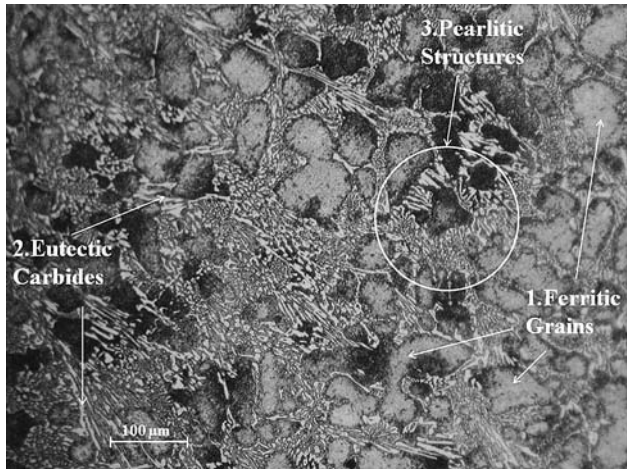

Fig. 7 Optical micrograph showing the microstructure of the alloy after H.T.B. 1: Ferritic grains 2: Eutectic carbides. 3: Pearlitic structures

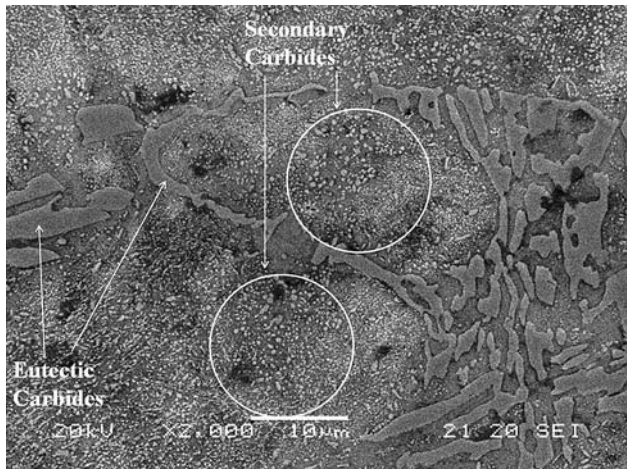

Fig. 8 SEM micrograph showing massive secondary carbide precipitation within the ferritic matrix after H.T.B

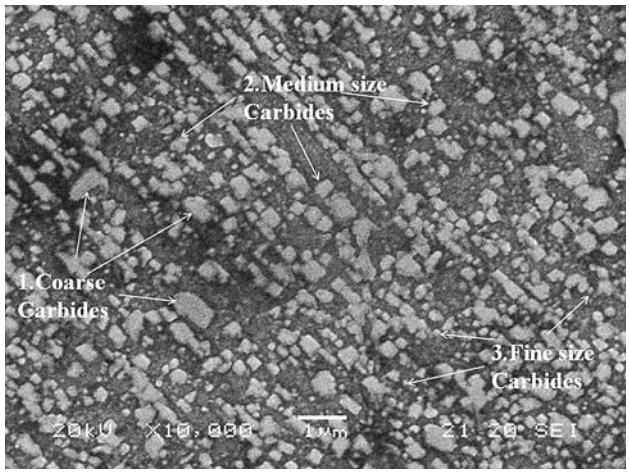

Fig. 9 Details of the circled area in Fig. 8. 1: Coarse/spheroidized M_7C_3 particles, 2: cubic $M_{23}C_6$ particles of medium size, 3: Fine size carbide particles

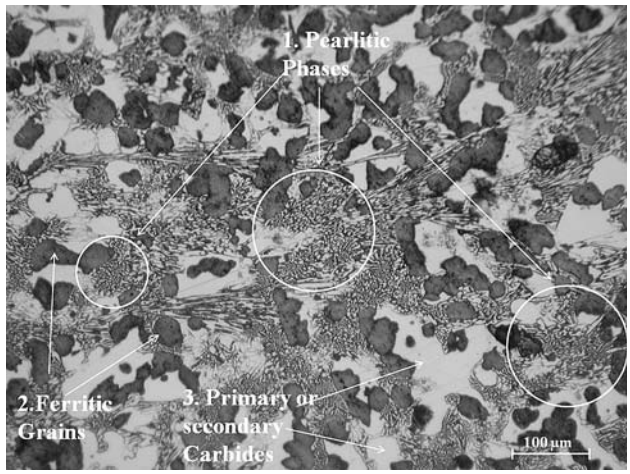

Fig. 10 Optical micrograph of the alloy after H.T.C. 1: Pearlitic structures, 2: Ferritic grains, 3: Spheroidized/slightly degraded primary eutectic carbides

categories, according to their size: coarse secondary carbide particles, medium size secondary carbide particles and fine size secondary carbide particles. This specific morphology significantly resembles to that observed by Powell and Bee (Ref 15), after prolonged isothermal treatment at the destabilization temperature (1273 °K). EDX analysis of the coarse carbide particles most likely suggests stoichiometries of the M_7C_3 type. This is attributed to the fact that during annealing some of the previously formed $M_{23}C_6$ secondary carbides (H.T.A) have been transformed into the thermodynamically more stable M_7C_3 type. The EDX analysis of the medium size carbides revealed stoichiometry of the $M_{23}C_6$ type. The technique could not provide reliable results for the fine size carbide particles due to their extremely small size. The presence of other carbide stoichiometries, such as M_3C and M_6C, is also possible (Ref 1, 8, 12-20).

Hardness values were of the order of 55 ± 4 HRC. The observed reduction, as compared with hardness after H.T.A, is mostly attributed to the formation of pearlitic/ferritic phases that have lower hardness than martensite. It has been reported that subcritical heat treatments, in general, lower, the abrasion wear resistance (Ref 1-8).

3.4 Heat Treatment C

The prolonged duration of this heat treatment, dramatically alters the initial as-cast microstructure, as observed in Fig. 10. The microstructure of the as-cast structure (austenite and eutectic carbides) has been extensively replaced by new phases. In Fig. 10, three different microconstituents can be distinguished, marked 1, 2, and 3. Microconstituent 1 has pearlitic structure. The extensively etched dark areas are ferrite microconstituent. Lastly, the identification of the remaining non-etched phase 3 could lead to confusing assumptions as microconstituent 3 could consist of either secondary carbides or spheroidized primary/degraded carbide structures. Further examination with SEM was undertaken, in order to clarify the identity of the carbide blocks. Figure 11 shows the structure of the material under a high magnification (×4000). No secondary carbide formation, at least of the $M_{23}C_6$ or similar stoichiometry, was observed. White etched areas correspond to ferrite grains. EDX analysis on the blocky-shaped carbides revealed

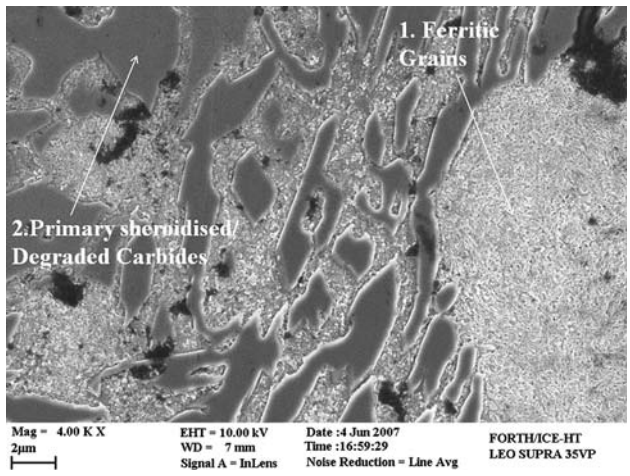

Fig. 11 SEM micrograph of the alloy after H.T.C. 1: ferrite, 2: spheroidized/slightly degraded carbide

compositions with M:C ratios slightly higher than 7:3. This indication could mean that the overall transformation mechanism of the primary M_7C_3 combines spheroidization and degradation to M_3C/M_6C. It is considered that the energy offered to the system by H.T.C is not sufficient to encourage either the formation of new carbide phases or the transformation into new carbides phases. Yet, the enhancement of the diffusion processes can cause a decrease in the interfacial energy by the spheroidizing process and the formation of outer layers of degraded carbide phases. These observations constitute a different approach to that proposed by Wang et al. (Ref 13) according to which prolonged (>16 h) annealing at similar temperatures (560 °C) have led to the formation of Cr-rich secondary carbides of the $M_{23}C_6$ type and perlitic structures. At intermediate annealing times (5, 10, and 15 h), martensite of different, in case, extent was formed. A possible reason for these differences could be the different chromium content (15wt.%), which could affect the martensitic transformation temperatures as well as the Cr/C ratio in the carbide phase. Further examination with XRD confirmed the presence of ferrite and carbide phases as well as the absence of

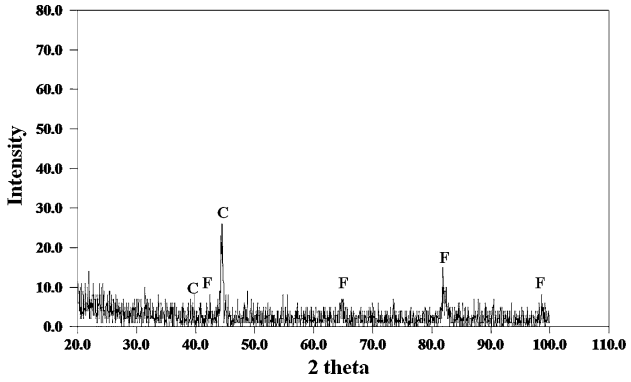

Fig. 12 XRD spectrum of the alloy after H.T.C. F: ferrite, C: M_7C_3

martensite (Fig. 12). As mentioned previously, it is difficult to distinguish between the different potential carbide candidate phases (M_7C_3, $M_{23}C_6$, M_6C, M_3C, Fe_3C, etc.) due to overlapping of the respective peaks. Nevertheless, EDX analysis supports the predominance of a stoichiometry close to M_7C_3.

Hardness measurements gave a mean value of 43 ± 5 HRC that is slightly lower than in the as-cast condition. This decrease is owing to the extensive transformation to pearlite as well as the spheroidizing. The lack of secondary carbide precipitation, the spheroidizing of the primary particles, and the extensive presence of pearlite/ferrite resulted in hardness values lower than those (51-60 HRC) measured by Wang et al. (Ref 13). As aforementioned, subcritical heat treatments reduce the abrasion wear resistance (Ref 1-4).

3.5 Heat Treatment D

The homogenization/destabilization (austenitization) heating and air quenched stage, resulted in notable alterations of the microstructure in comparison with previous cases. Figure 13 illustrates the microstructure of the alloy after H.T.D. Two main microconstituents are discerned: the eutectic carbide/austenite microconstituent and the acicular martensitic plate/retained austenite microconstituent. Areas of pearlitic morphologies are also identified. Additional SEM examination revealed the formation of spheroid secondary carbide particles of average diameter of 200 nm (Fig. 14 and 15). As can be seen in Fig. 14 and 15 the formation of the secondary carbide particles is almost exclusively initiated, progressed, and integrated within the austenite matrix. Limited, yet not negligible, however association of their formation with the periphery of the primary carbide phases can be recognized. XRD analysis proved difficult to clearly identify the involved carbide phases due to overlapping. Nevertheless, EDX analysis on the secondary carbide phase (as well as the primary carbide phase) revealed compositions close to the M_7C_3 stoichiometry. XRD analysis of the material identified the presence of martensite, carbides (mainly M_7C_3 according to EDX), and austenite (Fig. 16). The formation of martensite is a result of M_s increase due to extensive alloying element depletion caused by the secondary carbide formation.

It should be noticed that several workers (Ref 11-16) have reported that isothermal destabilization heat treatment leads to the formation of secondary carbide particles of the type of $M_{23}C_6$. The absence of secondary $M_{23}C_6$ in the present effort could be attributed to the fact that the alloy had been previously tempered by H.T.C. Thus the initial microstructure had

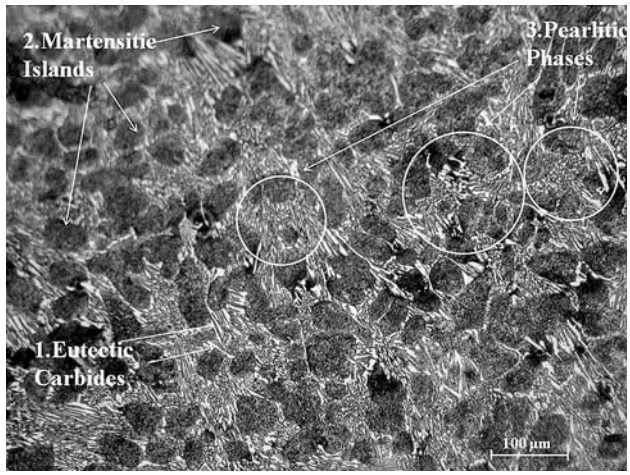

Fig. 13 Optical micrograph of the alloy after H.T.D. 1: eutectic carbides, 2: martensite, 3: pearlitic morphologies

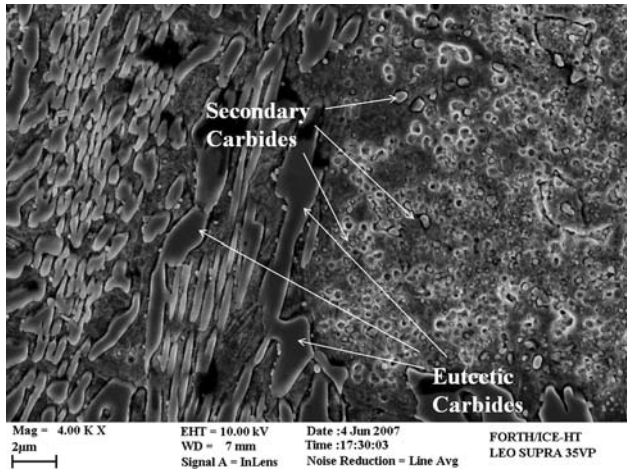

Fig. 14 SEM micrograph of the alloy after H.T.D showing excessive precipitation of secondary carbide particles within the martensitic matrix

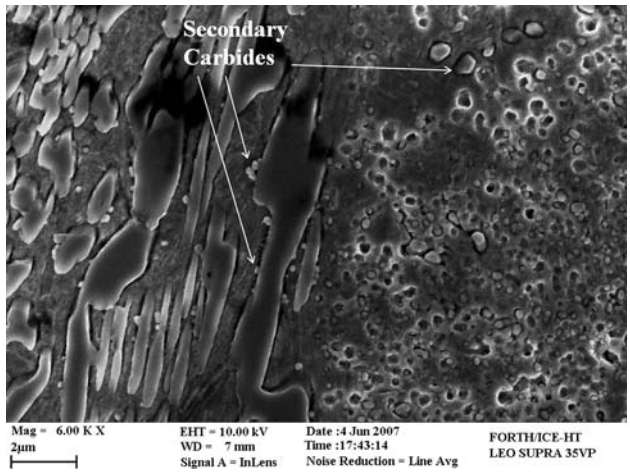

Fig. 15 SEM micrograph of the alloy after H.T.D presenting occasional precipitation of secondary carbide particles close in the vicinity of the primary eutectic carbide plates

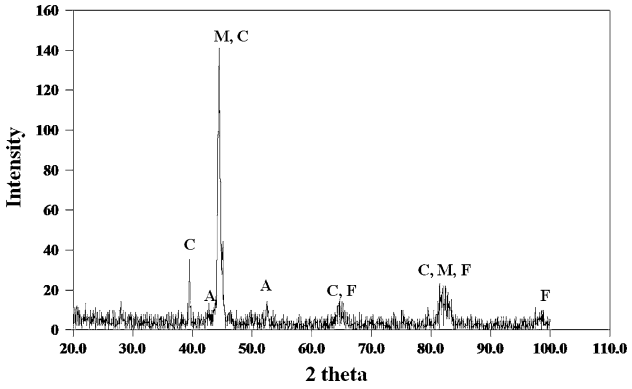

Fig. 16 XRD spectra of the alloy after heat treatment D. A: austenite, M: martensite, F: ferrite, C: M_7C_3 eutectic carbides

significantly altered. Spheroidized large M_7C_3 carbide particles (after H.T.C) are very stable, thus unlikely to be dissolved during destabilization, unless outer layers of degraded carbide forms are present which is the case in this specific treatment. In any case, the remaining Cr-poor, martensitic matrix is more likely to transform to a Cr-poorer carbide (such as M_7C_3) than a Cr-richer carbide (such as $M_{23}C_6$). This assumption is compatible with Powell and Laird's (Ref 16) findings reported in the introduction. Closer examination of the morphology of the primary eutectic carbides showed that the spheroidized (H.T.C) eutectic carbide particles, partially regained their initial shape and morphology. This is attributed to the dissociation of the unstable outer layers of degraded carbide forms with concomitant formation of some secondary carbide particles close to the eutectic phase, as shown in Fig. 15.

Hardness evaluation resulted in a mean value of 62 ± 4 HRC. These values indicate a significant increase in hardness, as compared with H.T.C, that is associated with the martensite formation and the secondary carbide precipitation. As a destabilization heat treatment, H.T.D should lead to improvement of the abrasion wear resistance in general (Ref 1-8).

To summarize, heat treatment D (H.T.D) that applies destabilization after subcritical heat treatment attains an increase in the hardness of the white iron and possibly an increase in the wear abrasion resistance as compared to the conventional destabilization—subcritical heat treatment (H.T.B). This is a result of the different microstructures obtained. The effect of the heat treatments on the wear resistance will be examined in detail, in a forthcoming publication.

4. Conclusions

- The initial as-cast structure of a high-chromium white iron consisted of primary austenitic dendrites and a eutectic mixture of M_7C_3/austenite. Cr depletion of the matrix in the close vicinity of the carbide particles had led to their engulfment by a thin martensite layer.
- The destabilization heat treatment A (H.T.A) drastically altered the microstructure, leading to extensive precipitation of cubic $M_{23}C_6$ carbide particles within the matrix. The latter was transformed into martensite. The hardness considerably increased.
- The subcritical heat treatment following H.T.A (both treatments compose heat treatment B—H.T.B) led to the transformation of the martensitic matrix to pearlite structures. The overall secondary carbide particle distribution was notably altered either by coarsening/transforming the previously precipitated carbide particles or by the formation of new finer carbide particles. The hardness slightly decreased.
- The subcritical heat treatment (H.T.C) drastically changed the microstructure of the as-cast alloy, leading to the formation of ferritic/pearlitic structures and the spheroidizing/slight degradation of the primary eutectic carbide particles. The hardness considerably decreased.
- The homogenization/austenitization and subsequent quenching treatment followed H.T.C (both treatments compose heat treatment D—H.T.D) led to an extensive formation of secondary spheroid M_7C_3 particles within the primary austenitic phase. The latter was mainly transformed into martensite. The hardness increased significantly.

Acknowledgment

The authors would like to acknowledge the Greek Modern Castings (GMC) S.A foundry for their kind assistance in the preparation of the examined alloy.

References

1. C.P. Tabrett, I.R. Sare, and M.R. Ghomashchi, Microstructure-Property Relationships in High Chromium White Iron Alloys, *Int. Mater. Rev.*, 1996, **41**(2), p 52–89
2. K.-H. Zum Gahr and G.T. Eldis, Abrasive Wear of White Cast Irons, *Wear*, 1980, **64**, p 175–194
3. C. Çetinkaya, An Investigation of the Wear Behaviours of White Cast Irons Under Different Compositions, *Mater. Des.*, 2006, **27**, p 437–445
4. Y. Matsubara, N. Sasaguri, K. Shimizu, and S.K. Yu, Solidification and Abrasion Wear of White Cast Irons Alloyed with 20% Carbide Forming Elements, *Wear*, 2001, **250**, p 502–510
5. S. Turenne, F. Lavallee, and J. Masounave, Matrix Microstructure Effect in the Abrasion Resistance of High Chromium White Cast Iron, *J. Mater. Sci.*, 1989, **24**, p 3021–3028
6. C.P. Tabrett and I.R. Sare, Effect of High Temperature and Sub-Ambient Treatments on the Matrix Structure and Abrasion Resistance of a High-Chromium White Iron, *Scr. Mater.*, 1998, **38**(12), p 1747–1753
7. M. Durand-Charre, *Microstructure of Steels and Cast Irons*, Springer-Verlag, New York LLC, April 2004, ISBN-13: 9783540209638
8. C.P. Tabrett and I.R. Sare, The Effect of Heat Treatment on the Abrasion Resistance of Alloy White Irons, *Wear*, 1997, **203–204**, p 206–219
9. C.P. Tabrett and I.R. Sare, Fracture Toughness of High-Chromium White Irons: Influence of Cast Structure, *J. Mater. Sci.*, 2000, **35**, p 2069–2077
10. S.K. Hannes and J.D. Gates, A Transformation Toughening White Cast Iron, *J. Mater. Sci.*, 1997, **32**, p 1249–1259
11. J. Asensio, J.A. Pero-Sanz, and J.I. Verdeja, Microstructure Selection Criteria for Cast Irons with More than 10 wt% Chromium for Wear Applications, *Mater. Charact.*, 2003, **49**, p 83–93
12. J. Wang, C. Li, H. Liu, H. Yang, B. Shen, S. Gao, and S. Huang, The Precipitation and Transformation of Secondary Carbides in a High Chromium Cast Iron, *Mater. Charact.*, 2006, **56**, p 73–78
13. J. Wang, R.L. Luo, Z.P. Sun, C. Li, H.H. Liu, H.S. Yang, B.L. Shen, and S.J. Huang, Influence of Secondary Carbides Precipitation and Transformation on Hardening of a 15Cr–1Mo-1.5 V White Iron, *Mater. Charact.*, 2005, **55**, p 234–240
14. M.X. Zhang, P.M. Kelly, and J.D. Gates, The Effect of Heat Treatment on the Toughness Hardness and Microstructure of Low Carbon White Cast Irons, *J. Mater. Sci.*, 2001, **36**, p 3865–3875

15. G.L.F. Powell and J.V. Bee, Secondary Carbide Precipitation in an 18 wt% Cr–1 wt% Mo White Iron, *J. Mater. Sci.*, 1996, **31**, p 707–711
16. G.L.F. Powell and G. Laird II, Structure, Nucleation, Growth and Morphology of Secondary Carbides in High Chromium and Cr-Ni White Irons, *J. Mater. Sci.*, 1992, **27**, p 29–35
17. A. Wiengmoon, T. Chairuangsri, A. Brown, R. Brydson, D.V. Edmonds, and J.T.H. Pearce, Microstructural and Crystallographical Study of Carbides in 30 wt% Cr Cast Irons, *Acta Mater.*, 2005, **53**, p 4143–4154
18. S.D. Carpenter and D. Carpenter, X-ray Study of M_7C_3 Carbide Within a High Chromium White Iron, *Mater. Lett.*, 2003, **57**, p 4456–4459
19. J.T.H. Pearce and D.W.L. Elwell, Duplex Nature of Eutectic Carbides in Heat Treated 30% Chromium Cast Iron, *J. Mater. Sci. Lett.*, 1986, **5**, p 1063–1064
20. J.T.H. Pearce, Examination of M_7C_3 Carbides in High Chromium Cast Iron Using Thin Foil Transmission Electron Microscopy, *J. Mater. Sci. Lett.*, 1983, **2**, p 428–432
21. A. Inoque and T. Masumoto, Carbide Reactions ($M_3C => M_7C3 => M_{23}C_6 => M_6C$) During Tempering of Rapidly Solidified High Carbon Cr-W and Cr-Mo Steels, *Metall. Transact. A*, 1980, **11A**, 739–747
22. S.D. Carpenter, D. Carpenter, and J.T.H. Pearce, XRD and Electron Microscope Study of a Heat Treated 26.6% Chromium White Iron Microstructure, *Mater. Chem. Phys.*, 2007, **101**, p 49–55
23. Z. Sun, R. Zuo, C. Li, B. Shen, J. Yan, and S. Huang, TEM Study on Precipitation and Transformation of Secondary Carbides in 16Cr-1Mo-1Cu White Iron Subjected to Subcritical Treatment, *Mater. Charact.*, 2004, **53**, p 403–409